THE ASTROPHYSICAL JOURNAL, 552:473–483, 2001 May 10
© 2001. The American Astronomical Society. All rights reserved. Printed in U.S.A.

BARYONS IN THE WARM-HOT INTERGALACTIC MEDIUM

ROMEEL DAVÉ[1]
Steward Observatory, University of Arizona, Tucson, AZ 85721; rad@as.arizona.edu
RENYUE CEN AND JEREMIAH P. OSTRIKER
Princeton University Observatory, Princeton, NJ 08544; cen@astro.princeton.edu, jpo@astro.princeton.edu
GREG L. BRYAN[1]
Department of Physics, Massachusetts Institute of Technology, Cambridge, MA 02139; gbryan@alcrux.mit.edu
LARS HERNQUIST
Harvard-Smithsonian Center for Astrophysics, Cambridge, MA 02138; lars@cfa.harvard.edu
NEAL KATZ
Department of Astronomy, University of Massachusetts, Amherst, MA 01003; nsk@kaka.phast.umass.edu
DAVID H. WEINBERG
Department of Astronomy, Ohio State University, Columbus, OH 43210; dhw@astronomy.ohio-state.edu
AND
MICHAEL L. NORMAN AND BRIAN O'SHEA
Astronomy Department, University of Illinois at Urbana-Champaign, Urbana, IL 61801; norman@ncsa.uiuc.edu, bwoshea@ncsa.uiuc.edu
Received 2000 July 15; accepted 2000 December 22

ABSTRACT

Approximately 30%–40% of all baryons in the present-day universe reside in a warm-hot intergalactic medium (WHIM), with temperatures in the range $10^5 < T < 10^7$ K. This is a generic prediction from six hydrodynamic simulations of currently favored structure formation models having a wide variety of numerical methods, input physics, volumes, and spatial resolutions. Most of these warm-hot baryons reside in diffuse large-scale structures with a median overdensity around 10–30, not in virialized objects such as galaxy groups or galactic halos. The evolution of the WHIM is primarily driven by shock heating from gravitational perturbations breaking on mildly nonlinear, nonequilibrium structures such as filaments. Supernova feedback energy and radiative cooling play lesser roles in its evolution. WHIM gas may be consistent with observations of the 0.25 keV X-ray background without being significantly heated by nongravitational processes because the emitting gas is very diffuse. Our results confirm and extend previous work by Cen & Ostriker and Davé et al.

Subject headings: cosmology: observations — intergalactic medium — large-scale structure of universe — methods: numerical

1. INTRODUCTION

Observations indicate that most of the baryonic matter in the universe does not reside in galaxies. At high redshifts ($z \gtrsim 2$), the overwhelming majority of baryons are in a diffuse, photoionized intergalactic medium (IGM), observable as H I absorption lines in the spectra of distant quasars (Cen et al. 1994; Zhang, Anninos, & Norman 1995; Miralda-Escudé et al. 1996; Hernquist et al. 1996). The baryonic density inferred from these observations (Rauch et al. 1997) is in good agreement with nucleosynthesis arguments based on observed deuterium abundances (Tytler, Fan, & Burles 1996). However, by redshift zero the total baryonic component, inferred from H I absorption, gas and stars in galaxies, and other observations, has declined to a level small compared to that seen at high redshift and expectations from nucleosynthesis (Persic & Salucci 1992; Fukugita, Hogan, & Peebles 1998). Thus the question arises, where are the baryons at the present epoch?

By the current epoch, hierarchical structure formation has produced deep potential wells into which the baryons accrete, thereby moving a significant portion of the baryons from the IGM into stars, galaxies, groups, and clusters. These complex evolutionary processes can now be modeled directly using cosmological hydrodynamic simulations, enabling an investigation into the location and phase of baryonic constituents in the present-day universe, and suggesting possible avenues for their direct detection.

These hydrodynamic simulations of structure formation indicate that baryons in the universe reside in four broad phases, defined by their overdensity $\delta \equiv \rho/\bar{\rho} - 1$ (where $\bar{\rho}$ is the mean baryonic density) and temperature T:

1. *Diffuse*: $\delta < 1000$, $T < 10^5$ K. Photoionized intergalactic gas that gives rise to Lyman alpha absorption.
2. *Condensed*: $\delta > 1000$, $T < 10^5$ K. Stars and cool galactic gas.
3. *Hot*: $T > 10^7$ K. Gas in galaxy clusters and large groups.
4. *Warm-hot*: $10^5 < T < 10^7$ K. The "warm-hot intergalactic medium" (WHIM), discussed here.

Cen & Ostriker (1999; hereafter CO99) and Davé et al. (1999; hereafter DHKW) predicted that a sizeable fraction of all baryons at the present epoch reside in this last warm-hot phase (see Fig. 2 of CO99 and Fig. 12 of DHKW). Such a reservoir has significant implications for producing an accurate census of baryons for comparison with nucleosynthesis arguments (e.g., Fukugita et al. 1998) because gas at these temperatures and densities is difficult to detect in either absorption or emission, as we discuss in § 6.

[1] Hubble fellow.

In this paper we study the nature and evolution of warm-hot gas in a ΛCDM universe, using a suite of cosmological hydrodynamic simulations having a wide range of numerical and physical parameters. The purpose of this paper is to ask how robust simulation predictions are to these parameters, to examine the physical state of warm-hot gas in the universe, and to investigate constraints on warm-hot gas from soft X-ray background observations.

In § 2 we briefly describe the simulations used. The evolution of diffuse gas at high redshift into condensed, hot, and WHIM gas at the present epoch is quantified in § 3. Our primary result, presented in § 4, is that the WHIM accounts for a significant fraction ($\sim$30%–40%) of the baryonic mass at $z = 0$, regardless of variations in spatial resolution, input physics, or hydrodynamic algorithm. This is because the evolution of the WHIM is driven primarily by shock heating of gas falling into gravitationally generated potential wells, a process that is well-understood and modeled, and only secondarily by processes such as supernova feedback, radiative cooling, and photoionization. Furthermore, most of the WHIM gas is at relatively low overdensities, so shock heating of intergalactic gas occurs during flows onto nonequilibrium large-scale structures such as filaments. The majority of warm-hot gas is found outside of virialized objects such as galactic halos and galaxy groups. The low overdensities explain why radiative cooling and supernova heating do not drive its evolution, and why the presence of this component probably does not violate constraints from the X-ray background, as we show in § 5. Finally, we briefly discuss strategies for direct detection of this gas, noting that the easiest place to detect emission from WHIM gas is relatively close to galaxies, where it is dense, even though most of the warm-hot baryons are not in these regions. In summary, the WHIM is a robust and generic prediction of currently popular hierarchical structure formation models, and it contains roughly one-third of all baryons in the universe today.

2. SIMULATIONS

We use six cosmological hydrodynamic simulations of randomly selected volumes in Λ-dominated cold dark matter (CDM) universes, employing three different numerical techniques, with a range of physical and numerical parameters. These parameters are summarized in Table 1. Simulations run with parallel tree smoothed particle hydrodynamics (PTreeSPH; Davé, Dubinski, & Hernquist 1997) are labeled D1 and D2, simulations run with total variation diminishing particle-mesh (TVD-PM; Ryu et al. 1993) are labeled C1 and C2, and simulations using adaptive mesh refinement (AMR; Bryan 1999) are labeled B1 and B2. The cosmology chosen is close to the "concordance model," which is in agreement with a wide variety of observations (Bahcall et al. 1999).

For our purposes, the significant inputs are the variations in spatial resolution (1–200 h^{-1} kpc), baryonic mass resolution (2×10^7–10^9 $M_\odot$), box size (11.11–100 h^{-1} Mpc), input physics, and hydrodynamic algorithms. D1 and D2 are high spatial resolution Lagrangian (particle-based) simulations, C1 and C2 are Eulerian simulations employing the total variation diminishing (TVD) scheme having lower spatial and higher mass resolution, and B1 and B2 are high-resolution adaptive-mesh simulations based on the piecewise parabolic method (note the exceptional resolution of ~ 1 h^{-1} kpc achieved by AMR in the high-density regions). All simulations except B1 include radiative cooling from H and He, photoionization heating, and star formation; B1 includes none of these. Simulations C1, C2, and B2 also include metal-line cooling, with the metallicity determined self-consistently from supernova output. All simulations use a Λ-dominated cold dark matter universe, having similar power at cluster and galaxy scales. B2 has only been evolved to $z = 0.75$, but this will be sufficient to indicate the relevant trends.

3. EVOLUTION OF INTERGALACTIC GAS

Figure 1 shows the evolution of the baryonic mass fraction in the four phases described above. The four panels show results from simulations D1, D2, C1, and C2. Despite differences in simulation volume, resolution, and numerical method, the evolution of various phases is qualitatively similar. At high redshift ($z \gtrsim 2$), the dominant fraction of baryons resides in diffuse gas (Fig. 1, *dashed lines*), giving rise to Lyα forest absorbers, as has been explored in detail elsewhere (see Rauch 1998 for a review). As structure forms, diffuse gas is shock heated, producing warm-hot gas (*solid lines*). Gas that is driven to higher densities by gravitational instability is able to cool into the condensed phase (*dotted lines*) and form stars. At lower redshifts ($z \lesssim 2$), large potential wells are produced that shock heat gas to $T > 10^7$ K, giving rise to hot cluster gas (*dot-dashed curves*). Nevertheless, at the present epoch, the total fraction of baryons in clusters is small.

Figure 1 shows that the fraction of diffuse baryons at the present epoch is between 20% and 40%, the fraction of

TABLE 1

SIMULATION PARAMETERS

Simulation	Code	Ω	Ω_Λ	n	Ω_b	H_0	σ_8	L[a] (h^{-1} Mpc)	ϵ[b] (h^{-1} Mpc)	$m_{\rm bar}$[c] ($M_\odot$)	Physics[d]	$\Omega_{\rm WHIM}/\Omega_b$	$C_{\rm WHIM}$[e]
D1.....	PTreeSPH	0.4	0.6	0.95	0.0473	65	0.8	50	7	8.5×10^8	1, 4	0.30	244
D2.....	PTreeSPH	0.4	0.6	0.95	0.0473	65	0.8	11.11	3.5	1.1×10^8	1, 3, 4	0.29	405
C1	TVD-PM	0.37	0.63	0.95	0.049	70	0.8	100	200	1.6×10^8	1, 2, 3, 4	0.42	34
C2	TVD-PM	0.37	0.63	0.95	0.049	70	0.8	50	100	2.0×10^7	1, 2, 3, 4	0.37	106
B1	AMR	0.3	0.7	1.0	0.04	67	0.9	100	50	7.9×10^9	adiabatic	0.32	208
B2	AMR	0.3	0.7	1.0	0.04	67	0.9	100	1	9.9×10^8	1, 2, 3, 4	≈ 0.3[f]	≈ 400[f]

[a] Box size in comoving h^{-1} Mpc.
[b] Spatial resolution in comoving h^{-1} kpc; for PTreeSPH and AMR, this is the highest resolution achieved in dense regions.
[c] Baryonic mass resolution. In TVD-PM, this is the average mass per cell.
[d] 1: H, He cooling; 2: metal cooling; 3: photoionization; 4: star formation and feedback.
[e] Clumping factor of warm-hot gas at $z = 0$; see § 5.
[f] Values extrapolated from $z = 0.75$ to $z = 0$ based on a comparison with simulation B1.

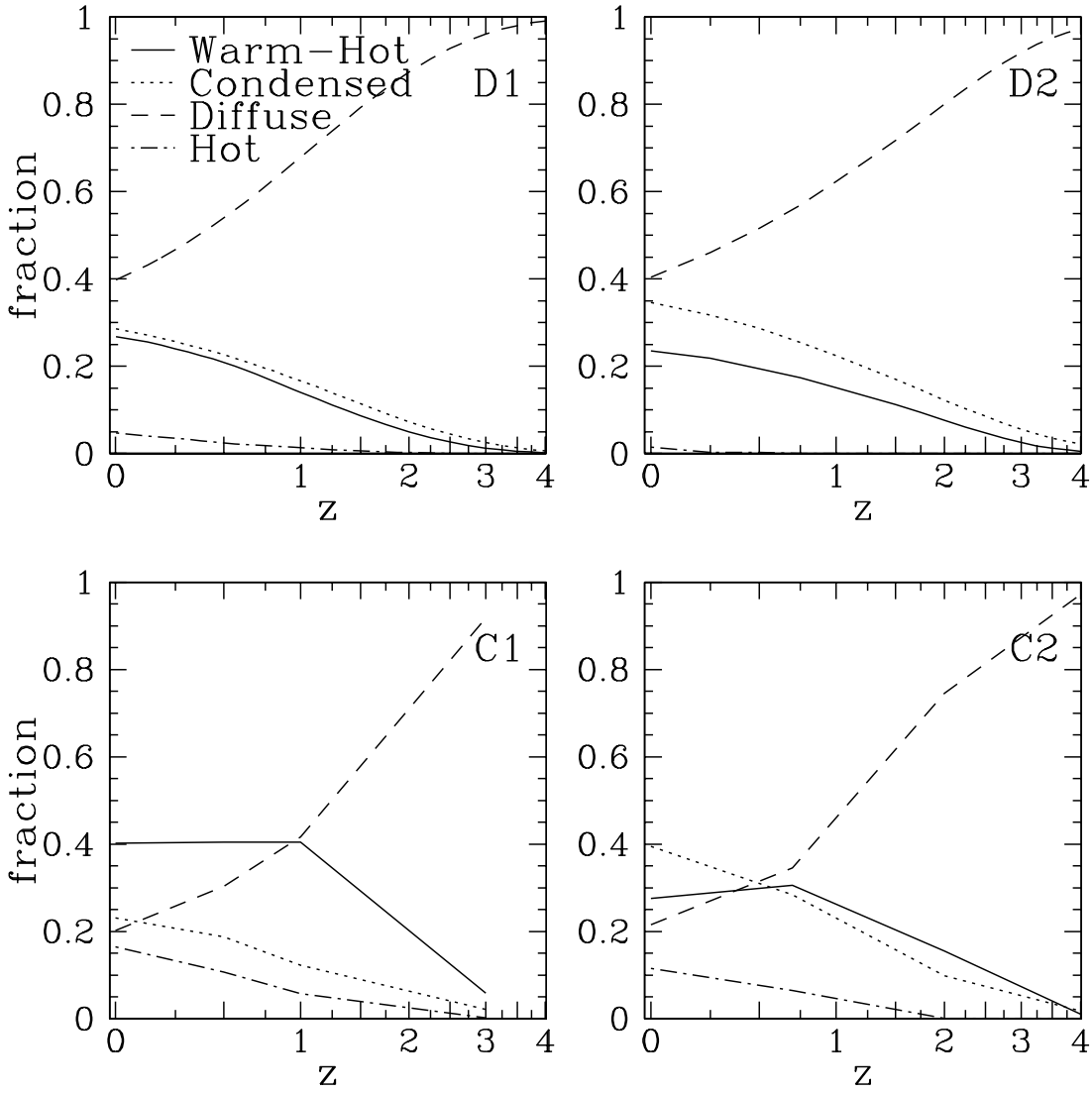

FIG. 1.—Evolution of mass fractions in four baryonic phases, in four simulations

warm-hot baryons is 30%–40%. Gravitationally bound baryons, i.e., those in stars, galactic gas, clusters, and intragroup media, make up the rest. Thus. baryons in the present-day universe are divided roughly equally among diffuse, warm-hot, and bound components.

While all the simulations are qualitatively similar, the exact distribution of gas in these phases is sensitive to details of the simulations. For instance, the condensed-phase fraction is sensitive to how gas cools and forms stars in these simulations, which in turn is significantly affected by resolution (since cooling and star formation $\propto \rho^2$). The effect of supernova feedback heating also depends strongly on resolution, as we discuss later. The growth of structure is affected by the amount of large-scale power present. In particular, the hot gas fraction in clusters is sensitive to cosmic variance, since it is dominated by the largest virialized objects in the volume. Other phases, including the warm-hot phase, are less sensitive to volume effects, as we show in § 4.1.

All things considered, it is not surprising that there are differences of up to a factor of 2 in the fractions in various phases at $z = 0$. While the differences may be significant, an investigation of their exact causes is beyond the scope of this work, although these differences offer clues to the physical processes driving WHIM evolution, as we explore in § 4.1. Rather, we focus on the remarkable qualitative consistency in the evolution of various gas phases, given the variety of simulation methodologies utilized.

For the condensed phase, a census of baryons in stars and cold gas estimates its mass fraction to be around 20% (Fukugita et al. 1998). This estimate does not include cold gas in small halos that may be below our simulation resolution limits, such as compact high-velocity clouds in the scenario of Blitz et al. (1999). However, The Arecibo H I Strip Survey indicates that the faint-end of the H I mass function is shallow, with a slope of 1.2 for $M_{\rm H\,I} > 10^{7.5}\,M_\odot$ (Zwaan et al. 1997). Such a slope implies that only a small fraction of neutral cold gas resides in halos below our resolution limit. For masses smaller than the Zwaan et al. limit, photoionization is expected to increasingly suppress the condensation of cold gas in dark matter potential wells (Quinn, Katz, & Efstathiou 1996; Thoul & Weinberg 1996). Thus, there may be some photoionized gas within these potential wells that would not be seen in H I surveys, although it is difficult to maintain such gas at high density over a Hubble time given the short cooling timescales.

The simulations shown generally produce somewhat higher values than those of Fukugita et al. (1998) for the condensed fraction, but there are uncertainties in the observed contributions from low-mass stars and supernova remnants. Of these simulations, C2 contains the largest fraction of condensed gas ($\sim 40\%$), while the rest are all lower, down to $\sim 25\%$ for simulation C1 (with the exception of B1, which of course has virtually no condensed gas, since it does not include cooling). While higher resolution simulations generally predict higher condensed fractions, it is not clear whether this is a physical prediction of our models or a result of numerical effects such as overcooling. Thus, in order to facilitate a less resolution-dependent comparison of the intergalactic components in these simulations, we fix the condensed fraction to be 20% and redistribute the remainder by proportionally increasing the fraction in other components. Our results are not qualitatively different if we do not carry out this redistribution. The question of why the "observed" condensed fraction is lower than predicted is important in its own right, but is beyond the scope of this paper.

4. THE WARM-HOT INTERGALACTIC MEDIUM

4.1. *Evolution of* $\Omega_{\rm WHIM}$

Figure 2 shows the evolution of the mass fraction of baryons in warm-hot gas, $\Omega_{\rm WHIM}/\Omega_b$, for our six simulations, with the condensed component fixed at 20%. Simulations C1 and C2 have the highest WHIM fractions, at 42% and 35% of baryonic mass, respectively, at $z = 0$. Simulations D1 and D2 have lower WHIM fractions at the present epoch, around $\sim 30\%$. Simulation B2 has only been evolved to $z = 0.75$, but its evolution closely mirrors that of the Lagrangian runs, so we expect that its WHIM fraction will also be $\sim 30\%$ by $z = 0$. These values are listed in Table 1. By the present epoch, all simulations have WHIM fractions within 50% of each other. Simulation B1 does not include radiative cooling, so it is an unphysical model that will only be used for comparison with B2.

We expect that the evolution of warm-hot gas is governed by shock heating of intergalactic gas onto large-scale structure, supernova feedback, and radiative cooling. Numerical

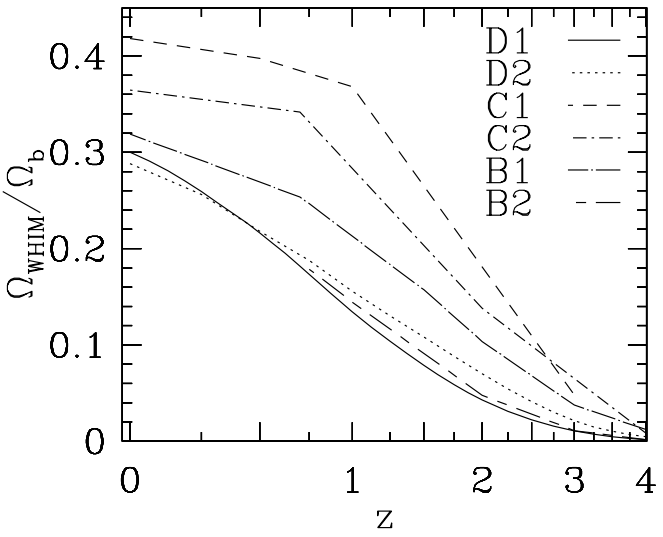

FIG. 2.— Evolution of $\Omega_{\rm WHIM}$ in our six simulations. For this comparison, the baryonic fraction in cold galactic gas and stars has been fixed at 20% in all simulations.

considerations such as resolution, volume, and hydrodynamic algorithm may also play a role. In this section we use case-by-case comparisons among our six simulations to examine how each of these processes affects WHIM evolution in our models.

All our simulations explicitly include the growth of structures and the accretion of gas onto those structures. The qualitative consistency of WHIM evolution in all our simulations, including simulation B1 without cooling or star formation, suggests that gravitational shock heating of gas falling on large-scale structures is the dominant heating mechanism for WHIM gas. This is an important point, as it suggests that all other differences between these simulations are of secondary importance.

The most obvious differences between models are that D1, D2 and B2 all predict similar WHIM evolution, while C1 and C2 have more WHIM gas. The primary distinction between these sets of simulations is spatial resolution. This manifests itself in various ways, since it affects gas cooling, the rate at which stars form, and the injection of supernova heat energy into intergalactic gas. To elaborate on this last point, high-resolution runs (D1, D2, and B2) deposit feedback energy (thermal only) locally in very high density regions where stars are forming, and thus it quickly radiates away, with virtually none of it being distributed into the intergalactic medium. Conversely, lower resolution runs (C1 and C2) deposit the same supernova energy over hundreds of kiloparsecs, resulting in a significant fraction of feedback energy escaping into diffuse regions where it cannot radiatively cool away. None of the simulations here are capable of resolving supernova-driven galactic winds through a multiphase interstellar medium, which are likely to be responsible for distributing energy and metals into the diffuse IGM (Mac Low 2000; Efstathiou 2000); thus, we are relying on heuristic modeling of these processes. As we discuss in § 4.2, it is in the distribution of feedback energy where resolution plays its most crucial role in predicting the evolution of WHIM gas.

First we examine the effect of radiative cooling. Simulation B1 has no cooling, whereas simulation B2 is a similar run with cooling (and is our highest spatial resolution run). Cooling has a greater effect at earlier times because intergalactic gas is denser then and thus can cool significantly. After $z \sim 3$, the rate of growth of the WHIM fraction is similar in B1 and B2, suggesting that WHIM gas is no longer affected by cooling. Even by $z = 0.75$, the difference between B1 and B2 is not large, indicating that cooling plays a minor role in the overall evolution of WHIM gas.

Eulerian codes resolve shock fronts better than smoothed particle hydrodynamics (SPH) in diffuse regions (Kang et al. 1994), because they have a higher density of resolution elements there, and in the case of the Eulerian codes discussed here, because they incorporate explicit shock capturing algorithms to resolve fronts over two cells. If a significant component of shock heating arises from small-scale shocks unresolved by SPH, Eulerian codes may produce higher temperatures. One might suspect that the difference between PTreeSPH runs and TVD-PM runs could be partially due to this effect. However, B2 captures small-scale diffuse shocks much better than the SPH runs, yet it has nearly the same WHIM fraction. So this cannot be a significant effect.

Simulation volume could also play a role in the amount of WHIM gas, since larger volumes contain larger pertur-

bations that can result in stronger gravitational shock heating. This may explain the difference between C1 and C2, whose box lengths differ by a factor of 2. However, D1 has a box length 5 times that of D2, yet their WHIM fractions are nearly identical at all times. Furthermore, B2 has twice the box length of D1, yet its WHIM fraction is in good agreement with D1 and D2. As we show in the next section, typical WHIM gas is at very moderate overdensities, and cosmic variance in that regime is typically small, in contrast to the hot IGM fraction, which is dominated by rare, massive objects (i.e., clusters) whose numbers are more sensitive to simulation volume.

It is possible that opposing effects are causing D1, D2, and B2 to be similar. For instance, D1 resolves shock fronts better than D2, perhaps resulting in more shock heating and making up for its lack of large-scale power. It is also possible that the adaptive refinement of B2 results in more cooling in shock fronts, compensating for its larger volume. However, unless all of these effects are of secondary importance, cancellations at the level we find here would require a remarkable coincidence.

The parameters of the underlying cosmological model are expected to have a nonnegligible effect on the WHIM component. The rate of structure evolution in large part determines how much shock heated gas is present at any epoch. While we have not sampled a range of cosmologies here, DHKW examined four cosmologies, namely ΛCDM, tilted CDM, cold + hot DM, and open CDM models, using numerical parameters similar to those of simulation D2. The differences between the WHIM fractions (called "shocked" gas in DHKW) in those models at the current epoch is comparable to the differences seen here due to other factors, as indicated by their Figure 12. Similarly, CO99 examined ΛCDM, cold + hot DM, and open CDM models, and also found broad consistency. Thus, while our quoted fractions may be specifically for a ΛCDM cosmology, our qualitative conclusions are unlikely to be highly sensitive to cosmology.

In summary, the evolution of $\Omega_{\rm WHIM}$ is qualitatively consistent among all simulations examined, and results in $\approx$30%–40% of baryons residing in the WHIM today. Radiative cooling, simulation volume, and algorithmic details do not significantly affect WHIM evolution in these runs.

4.2. *The Physics of WHIM Gas*

We now explore the physics that drives the formation and evolution of WHIM gas. A qualitative physical picture of WHIM gas can be obtained by examining Figure 3, which shows the location of gas in simulation C2 having $10^5 < T < 10^7$ K, with contours color-coded by density. WHIM gas is seen to primarily trace out filamentary large-scale structures. Like the intergalactic medium, WHIM gas

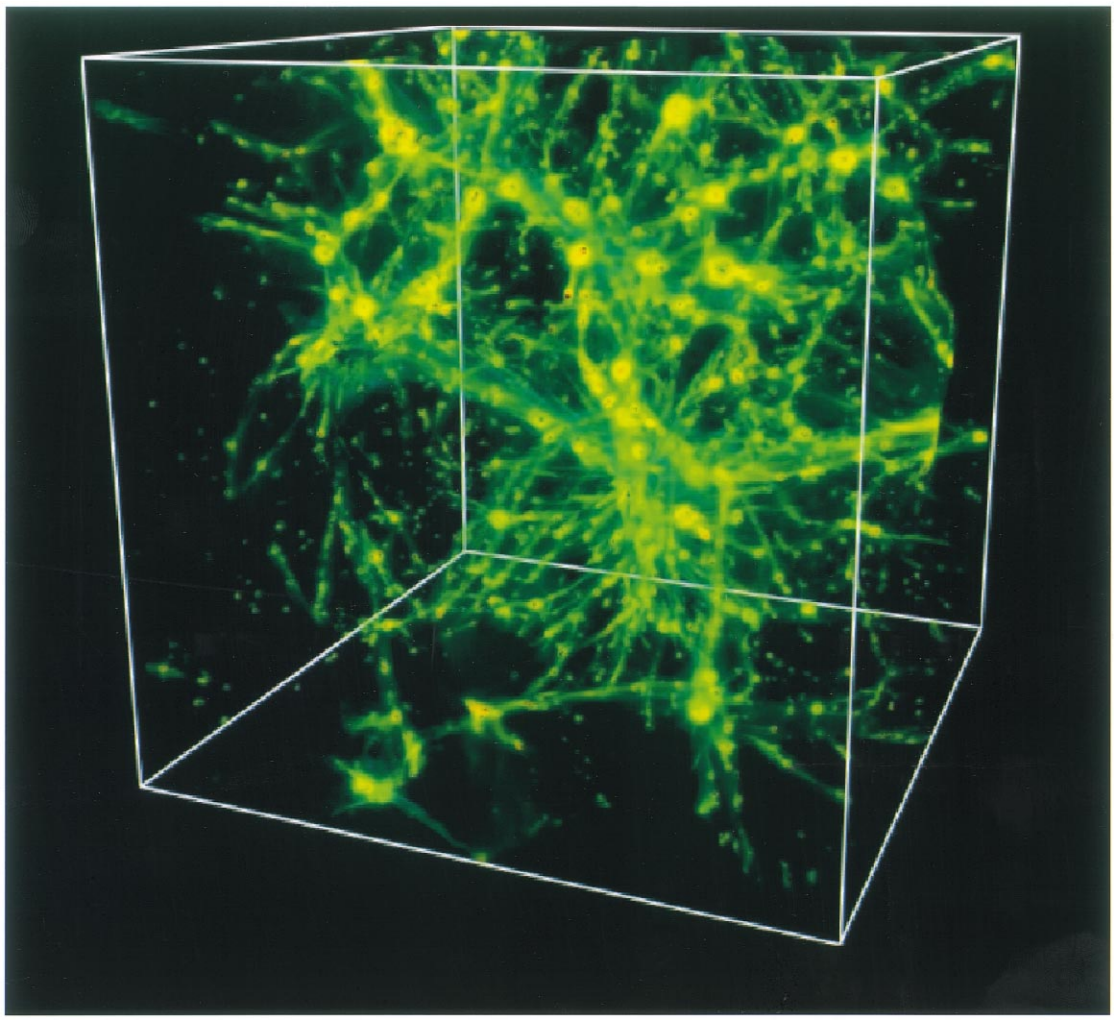

FIG. 3.—WHIM gas in simulation C2. Contours are color-coded by overdensity; green represents overdensity $\delta \sim 10$, while red shows $\delta \sim 10^4$.

does cluster around dense regions that are sites of galaxy formation. However, we show below that the majority of WHIM gas is contained in the filaments.

The top panel of Figure 4 quantifies the spatial distribution of WHIM gas in the universe. It shows a histogram of WHIM gas mass as a function of density for simulations D1, D2, C1, and C2. All four simulations consistently show that the dominant fraction of WHIM gas is at relatively low densities, with a peak around an overdensity of $\sim$10–30. Simulations B1 and B2 are not shown because B1 does not include cooling and B2 has only been evolved to $z = 0.75$. Still, B1 at $z = 0$ and B2 at $z = 0.75$ show peak overdensities of 18 and 21, respectively, so they are consistent with the other simulations. We see that 70%–80% of WHIM baryons lie in the overdensity range $5 < \delta < 200$, typical of filaments. Note that the densities in TreeSPH are computed slightly differently than in mesh-based runs; in the former, the density field is smoothed by the (variable) smoothing length of the particle, while in the latter the smoothing is fixed at the cell size. However, since in both cases the smoothing is done on scales smaller than the density variations, this is not expected to produce any systematic differences in the resulting densities.

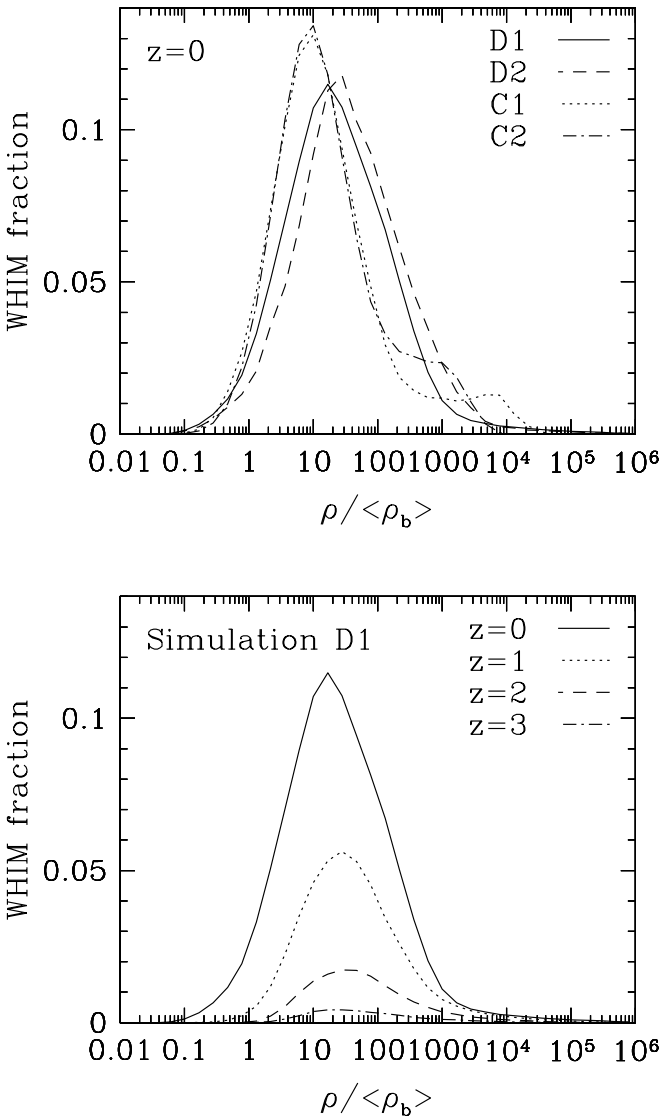

FIG. 4.—*Top*: Mass fraction of WHIM gas as a function of density at $z = 0$ in our simulations. *Bottom*: The same quantity at $z = 0$, 1, 2, and 3 in simulation D1.

The typical overdensities of WHIM gas are much smaller than that of matter contained in bound, virialized objects. A maximal estimate of the bound fraction of WHIM gas can be obtained as the fraction of WHIM gas with $\delta \gtrsim 60$, which is approximately the overdensity at the virial radius of an isothermal sphere in a ΛCDM cosmology. The mass fraction of WHIM gas with $\delta \gtrsim 60$ is $\approx$30% in our simulations. Clearly, some of this gas will not be bound, but rather infalling material. As an independent check, we use the group-finding algorithm SKID[2] (Spline Kernel Interpolative DENMAX) to identify bound warm-hot particles in simulation D1, and find a bound fraction of WHIM gas between $\sim$10% and $\sim$25%, depending on the linking length used (50–500 h^{-1} kpc). The lower end of this range probably corresponds to gas contained in galactic halos, although the extent of a galactic halo becomes ill-defined when it resides within a group or cluster. In summary, WHIM gas is mostly an intergalactic component, with a majority of it residing outside of virialized structures such as galaxies or groups. Note that coronal gas in galaxies also lies in the warm-hot temperature range, but it is a small fraction of the galactic baryonic mass (perhaps 10%; see, e.g., Blitz & Robishaw 2000), since most galactic baryons are tied up in stars and cold gas.

How can intergalactic gas be heated to $T > 10^5$ K without being bound in a massive virialized halo? One way would be if energy were added from nonthermal processes such as supernova feedback. However, this is not the driving process for WHIM gas in these simulations. Supernova feedback energy is added in all simulations shown in Figure 4, but in simulations D1, D2, and B2 the effect is negligible, since, as discussed above, feedback is added purely thermally into very dense regions, where it radiates away almost immediately and adds no heat to diffuse regions. Yet even in these high-resolution simulations, where supernovae add negligible heat to WHIM gas, the typical overdensities are smaller than those typical of virialized halos.

Supernova heating is, however, likely to be responsible for the somewhat lower overdensities in simulations C1 and C2 as compared to the higher resolution simulations, so its effect is nonnegligible. The differences cannot be due to other spatial resolution effects such as cooling, since C1 and C2 are themselves quite similar, as are D1 and D2. Instead, the lower spatial resolution in C1 and C2 results in significant supernova energy being deposited in intergalactic gas, as described in the previous section. This additional feedback heating raises the pressure of intergalactic gas and lowers the typical density. Furthermore, because supernova energy is not radiated away immediately, there is a small component of warm-hot gas in and around galaxies, seen as the high-density bump for C1 and C2 in Figure 4. R. Cen has recently run a simulation analogous to C2 except with no feedback, and finds WHIM distributions more along the lines of the TreeSPH and AMR simulations, further supporting the idea that supernova energy distribution represents the dominant difference between high and low spatial resolution runs.

[2] SKID is available at: http://www-hpcc.astro.washington.edu/TSEGA/tools/skid.html.

The effect of supernova heating can be roughly estimated by the following simple argument. Consider two extreme cases: one in which all supernova energy is deposited within dense regions where it immediately radiates away, and another in which supernova energy is distributed uniformly over all baryons in the universe. The former case is a reasonable approximation for the Lagrangian runs D1 and D2 and the high-resolution AMR run B2, while the latter is closer to the Eulerian runs C1 and C2 (although clearly a much more extreme case). In the former case, supernovae add no heat to WHIM gas. In the latter, the specific heat added per baryon yields a temperature increase of

$$\delta T_{\rm SN} = \frac{\Omega_* \rho_{\rm crit} \epsilon_{\rm SN}}{k_{\rm B} \bar{n}_{\rm H}} , \quad (1)$$

where Ω_* is the cosmic mass fraction in stars, $\rho_{\rm crit}$ is the critical density, $\epsilon_{\rm SN}$ is the specific energy output per unit mass of stars formed, and $\bar{n}_{\rm H}$ is the mean number density of H atoms. We take $\Omega_* = 0.1\Omega_b = 0.002h^{-2}$, and $\epsilon_{\rm SN} = 2.5 \times 10^{48}$ ergs g^{-1} $M_\odot$ from a Salpeter IMF with each supernova from a star with $M > 8$ $M_\odot$ outputting 10^{51} ergs. Then, $\delta T_{\rm SN} = 0.2$ keV $\approx 2 \times 10^6$ K. Assuming isentropic heat distribution, $\rho T^{3/2} = {\rm const}$, so gas with $T \approx 4 \times 10^6$ K (the maximum of the temperature distribution, as we show in Fig. 5) will have its density reduced by roughly a factor of 2 compared to the no-heating case. This is roughly the level of reduction seen in the Eulerian as compared to the Lagrangian runs. Clearly, this model is overly simplistic, since it would predict that all intergalactic gas has $T \gtrsim 10^6$ K, but it does roughly indicate the magnitude of the effect of supernova heating.

Note that there are no other heating processes in these simulations that contribute significantly to the WHIM. For instance, photoionization only heats gas to $\sim 10^4$ K. Any other heating process one could devise, such as cosmic rays or supernovae occurring in dwarf galaxies in voids, would add more pressure support to the gas, and thus would push the typical density of WHIM gas even lower. Thus, our simulations indicate that WHIM gas is heated to $T > 10^5$ K primarily by shock heating of gas accreting onto large-scale structure. These structures, typically filamentary, are *not* virialized or in dynamical equilibrium.

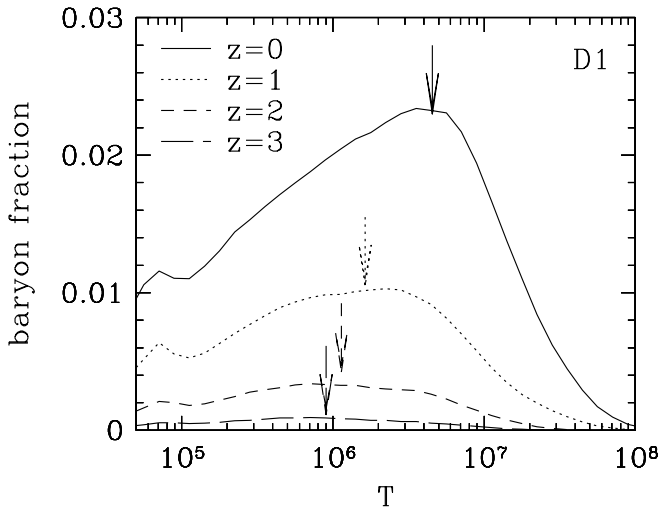

FIG. 5.—Mass fraction of baryons as a function of temperature in simulation D1, at $z = 0$ (*solid line*), $z = 1$ (*dotted line*), $z = 2$ (*short-dashed line*), and $z = 3$ (*long-dashed line*). The arrows indicate the predicted peak temperature from gravitational shock heating at various z, from eq. (2).

In the previous section we showed empirically that radiative cooling has a minor effect on WHIM evolution. This can be understood physically, given that warm-hot gas is typically at such low overdensities that it cannot collapse into virialized objects, and because of the metagalactic photoionizing background most intergalactic gas lies well within the optically thin regime (see DHKW, Fig. 10). Thus, typical WHIM gas is too diffuse to self-gravitate or self-shield, and has no way to achieve the densities required to make radiative processes important. Improving the numerical resolution of our simulations would not change this result, since it is based on simple physical arguments.

The bottom panel of Figure 4 shows a histogram of WHIM gas mass for the D1 model at $z = 0$, 1, 2, and 3 (*solid, dotted, dashed, and long-dashed lines, respectively*). There is a slight trend to higher overdensities at earlier times, since at early times the contribution from virialized structures is greater. This is because gas has not had time to accrete and shock on more diffuse structures, and the largest structures at earlier times have lower temperatures that can fall into the warm-hot range. Still, this is a minor effect; basically, the peak overdensity does not evolve significantly with redshift.

Figure 5 shows the temperature distribution of intergalactic gas with $T > 10^{4.5}$ K in simulation D1 at $z = 0$, 1, 2, and 3. The amount of gas at these warm-hot and hot temperatures grows with time, as seen from Figures 1 and 2. The temperature at the peak of the distribution grows in time as well, reflecting the fact that the universe contains hotter structures at later times. The peak temperature at all redshifts falls within the warm-hot range, and by $z = 0$ it is up to $\sim 4 \times 10^6$ K. Note that this is close to the temperature of the excess diffuse emission seen by Wang & McCray (1993) in *ROSAT* data. Figure 5 also shows that the mass of the WHIM component is insensitive to our somewhat arbitrary choice of 10^5 K as the defining lower temperature. A choice of $10^{4.5}$ K (as in DHKW) or even $10^{5.5}$ K would not drastically affect our conclusions.

An analytic estimate of the evolution of the peak temperature can be obtained by considering the temperature of intergalactic gas shock heated on mildly nonlinear large-scale structure. If the length scale going nonlinear at a given epoch is $L_{\rm nl}$, and the perturbation collapses on a timescale t, the resulting sound speed behind the shock will be $\sim L_{\rm nl}/t$. Given that the perturbation has taken a Hubble time to collapse, $t \sim H^{-1}$, where H is the Hubble constant at time t. The resulting postshock temperature is then (CO99)

$$T_{\rm nl} \propto c_{\rm nl}^2 = K(HL_{\rm nl})^2 , \quad (2)$$

where K is a constant, at any given epoch. The value of $T_{\rm nl}$, with $K = 0.3$, is shown at each redshift plotted in Figure 5 by the arrows above each curve. This value of K produces roughly the correct peak temperature at $z = 0$, and as can be seen from Figure 5, it is a reasonable fit to the peak temperature at higher redshifts, although it becomes progressively more difficult to identify a peak. This value of K also produces the correct evolution of the globally averaged temperature in simulations C1 and C2, as shown in CO99. Interestingly, this value is close to $K = 5/16$, which is the postshock sound speed of a strong shock. Thus, the evolution of the temperature distribution of WHIM gas is consistent with the interpretation that it is heated by

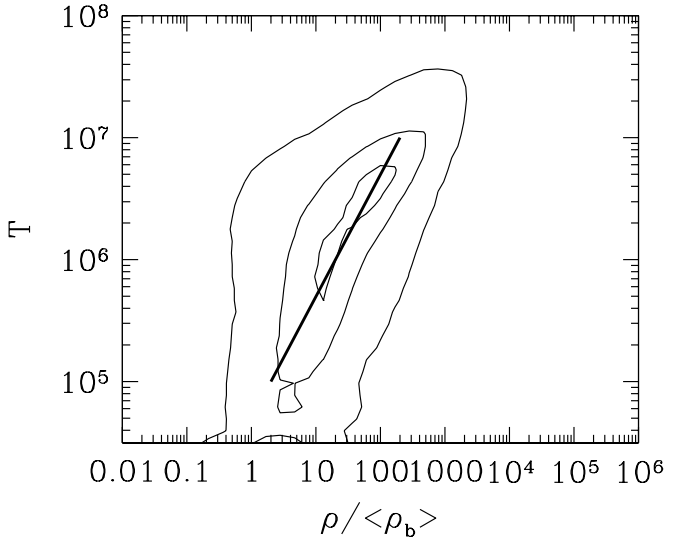

FIG. 6.— Contours in temperature and density for simulation D1 at $z = 0$, enclosing 10%, 50%, and 90% of the baryons in the range shown. Density and temperature are correlated in the WHIM regime. Thick line indicates a scaling of $\rho/\bar{\rho}_b = T/10^{4.7}$ in the warm-hot temperature range.

gravitationally induced shocks on mildly nonlinear large-scale structure. Since there is a wide range in the properties of the collapsing structures and therefore infall velocities, there is also a wide range in gas temperatures.

The temperature and density of WHIM gas are correlated. Figure 6 shows a contour plot of mass within the warm-hot range, as a function of density and temperature, for the D1 model at $z = 0$. The contour levels enclose 10%, 50%, and 90% of the mass in the temperature and density ranges shown in the plot. The thick line indicates an "equation of state" $\rho \propto T$ that provides a reasonable fit to gas in the range $10^5 < T < 10^7$ K. This relationship is different from that of diffuse gas, which typically has $\rho \propto T^{1.7}$, and the temperature-density relation of WHIM gas has much greater scatter. The higher temperature, different slope, and greater scatter all reflect the importance of shock heating as the dominant mechanism controlling the thermal properties of WHIM gas; the "equation of state" for diffuse gas, on the other hand, arises from the competition between photoionization and adiabatic cooling due to Hubble expansion (Hui & Gnedin 1997). Figure 6 also suggests that detecting WHIM gas in emission will be easier for gas that is at the highest end of the WHIM temperature range, since that gas will be both denser and hotter. However, the dominant portion of WHIM gas is at lower temperatures, which is perhaps most easily detected via absorption lines (Tripp, Savage, & Jenkins 2000).

5. CONSTRAINTS FROM THE SOFT X-RAY BACKGROUND

Gas with temperatures in the range $10^5 < T < 10^7$ K will emit thermally in the soft X-ray band. The extragalactic soft X-ray foreground (SXRB) flux at 0.1–0.4 keV is roughly $\sim$20–35 keV cm^{-2} s^{-1} sr^{-1} keV^{-1} (Warwick & Roberts 1998), although uncertainties are large because galactic coronal gas provides an increasing foreground to lower energies. At slightly higher energies ($\sim$1 keV), the XRB has been resolved nearly completely ($\sim$80%–90%) into point sources, mostly active galactic nuclei (AGNs; Mushotsky et al. 2000). Reasonable arguments then allow only a small contribution to the SXRB from diffuse gas, $\lesssim$4 keV cm^{-2} s^{-1} sr^{-1} keV^{-1} (Wu, Fabian, & Nusser 2000, hereafter WFN00). Direct extragalactic measurement of the 0.7 keV background from shadowing by the Magellanic bridge yields similar constraints (Wang & Ye 1996). Such a limit, in principle, places constraints on the number of baryons at warm-hot temperatures.

These limits were explored in two independent papers using similar methodologies, WFN00 and Pen (1999). Both papers argue that the standard picture of hierarchical formation of virialized objects results in a predicted SXRB that greatly exceeds the observed limits. They suggest that significant nongravitational heating, typically $\sim$1 keV per baryon, is required to reduce the density of warm-hot gas in virialized objects in order to satisfy the SXRB constraints. In this section we discuss these constraints in the context of WHIM gas, and find that our simulations paint a very different physical picture for soft X-ray emission than the models assumed in those two papers, in a way that can substantially lower the SXRB. The essential difference is one of density. Both WFN00 and Pen (1999) base their calculations on a Press-Schecter analysis, which assumes that all soft X-ray–emitting gas resides in virialized halos. In our simulations, WHIM gas resides primarily in lower density filamentary structures (see Figs. 3 and 4), and hence its SXRB emission is lower.

We can quantify this difference in typical WHIM density by considering the clumping factor of the emitting gas. If we define the clumping factor for gas component g as

$$C_g \equiv \frac{\langle \rho_g^2 \rangle}{\langle \rho_g \rangle^2}\,, \tag{3}$$

then the free-free emissivity from that component is

$$\epsilon_{\rm SXRB} \propto \langle \rho_g^2\, T_g^{0.5} \rangle \propto C_g\, \Omega_g^2\, T_g^{0.5}\,, \tag{4}$$

where ρ_g, Ω_g, $T_g \approx 10^6$ K, and C_g are the density, mass fraction, temperature, and clumping factor of the gas emitting in soft X-rays. The flux $j_{\rm SXRB}$ of soft X-ray background is then the emissitivity multiplied by path length $\sim \frac{1}{3} cH^{-1}$ (plus emission due to metal lines). WFN00 argue, sensibly, that it is predominantly warm-hot gas ($10^5 < T < 10^7$ K) that is responsible for soft X-ray emission. This means that the appropriate clumping factor C_g is that of *warm-hot* gas, $C_{\rm WHIM}$.

There are several ways to calculate $C_{\rm WHIM}$ in our simulations. One can directly calculate it from equation (3), which is the approach we use for our Eulerian simulations. For Lagrangian simulations, because each particle represents a different volume of gas, it becomes more numerically convenient to calculate $C_{\rm WHIM} \approx \xi_{\rm WHIM}(0)$, where $\xi_{\rm WHIM}(r)$ is the two-point correlation function of WHIM gas at radius r. The resulting $C_{\rm WHIM}$ values for our simulations at $z = 0$ are listed in Table 1. All simulations show clumping factors in the range $\sim$30–400. The smaller clumping factors in C1 and C2 arise directly because the WHIM gas is typically less dense in these models as compared to the other models because of greater supernova feedback energy deposited in the diffuse IGM, as explained in § 4.2. Of course, the assumption of a single WHIM temperature is also incorrect, since Figure 6 shows that ρ and T are correlated in the WHIM range; however, this is not the main source of discrepancy between the Pen (1999) prediction and ours.

Hydrodynamic simulations by Pen (1999) yielded a firm lower limit of $C_{\rm WHIM} \gtrsim 900$, assuming that the X-ray–

emitting gas traces the distribution of gas in galaxy halos. However, our simulations indicate that the spatial distribution of WHIM gas is quite different from that of galaxies. Figure 7 shows the autocorrelation function of WHIM gas ($\xi_{\rm WHIM}$) for simulation D1 (*solid line*) and D2 (*dashed line*), as well as the autocorrelation function of SKID-identified galaxies in simulation D1 ($\xi_{\rm galaxy}$, *dotted line*). At scales less than a few hundred kpc, $\xi_{\rm WHIM}$ flattens, indicating that WHIM gas does not cluster strongly on scales smaller than those typical of large-scale structures. Conversely, the galaxy correlation function continues as approximately a power law in to the resolution limit of our simulations.

Pen (1999) further derives that the observed SXRB requires $C \lesssim 60$, assuming that all baryons in the universe contribute to the SXRB (see his eq. [2]). In our simulations, only $\sim$30% of the baryons reside in the WHIM. From equation (4), we see that a reduction in Ω_g, the mean density of emitting gas, results in an increase in the maximum allowed clumping factor by $(\Omega_b/\Omega_{\rm WHIM})^2 \approx 10$. Thus, his analytically derived constraint translates to $C_{\rm WHIM} \lesssim 600$. Our clumping factors ($\lesssim$400) are consistent with his analysis, despite the fact that WHIM gas in our simulations undergoes almost no nongravitational heating.

WFN00 present a similar model to that of Pen (1999). They additionally allow some gas to cool below X-ray–emitting temperatures in the very centers of halos, but this has only a modest impact on their SXRB predictions because the cooling gas emits mostly in the X-ray continuum. A crude correction to their predicted SXRB based on our physical picture of WHIM gas would result in $j_{\rm SXRB}$ lowered by a factor of $C_{\rm WHIM}/C_{\rm galaxy}$, correcting for the fact that they use virialized objects (which we take as galaxies) instead of the true diffuse WHIM responsible for SXRB emission. Thus, we would naively predict a SXRB flux that is at least an order of magnitude lower than that predicted by WFN00, making it consistent with observed limits (see their Fig. 3). While this estimate does not account for potentially significant effects, such as the fact that the clumping factor of galaxies may be lower than that of galaxy groups responsible for SXRB emission in the WFN00 scenario (since there are many galaxies in a group), it does indicate that the physical picture presented here can result in large alterations in the predicted SXRB.

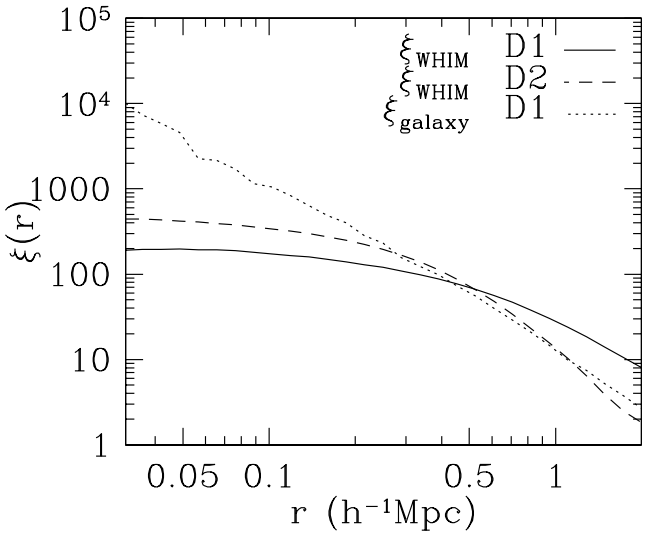

FIG. 7.—Two-point correlation functions for WHIM gas from simulations D1 (*solid line*) and D2 (*dashed line*), and for galaxies from simulation D1 (*dotted line*).

These arguments do not guarantee that the simulations are consistent with the observed SXRB. In particular, Table 1 taken at face value does not show clear convergence of the clumping factor. However, most of the range in Table 1 comes from comparing simulations in which supernova feedback has a large effect (C1 and C2) to those where it does not (D1, D2, and B2). Improving simulation resolution cannot result in much less supernova energy being deposited in the IGM, since in the latter cases it is already approaching zero. In any case, our simulations robustly predict that most WHIM gas is at densities lower than that of virialized halos (see Fig. 4), and this fact alone drastically alters the predicted SXRB from the calculations of Pen (1999) and WFN00. Note that the number density of galaxy groups in our simulation is not significantly different from that predicted by Press & Schecter (1974), but the density of soft X-ray–emitting gas within these groups is lower, and furthermore the total amount of warm-hot baryons in groups is smaller, since much of it still resides in diffuse large-scale structure. Our definition of the WHIM includes *all* baryons expected to contribute to the SXRB (i.e., having $10^5 < T < 10^7$ K), and thus there is no "additional component" of emission arising from groups. A more accurate determination of X-ray emission from these simulations, accounting for metallicity, instrumental bandpass, and numerical resolution issues, is detailed in recent works by Croft et al. (2001) and Phillips, Ostriker, & Cen (2001). These papers more explicitly show that the SXRB is not grossly overproduced in the simulations presented here, and furthermore that the WHIM is not the dominant source of SXRB photons.

Our results substantially weaken the case for nongravitational heating of the IGM, because they show that the physics of soft X-ray–emitting gas is very different from that assumed in Press-Schecter–based models. In our simulations, warm-hot gas acquires most of its energy gravitationally, but this shock heating occurs mainly in filaments rather than in virialized structures, and hence this gas remains at low overdensity. Furthermore, a substantial component of shock heated gas within halos cools to $T < 10^5$ K during the assembly of galaxies within a group, emitting its energy in Lyα and other atomic transitions rather than in the X-ray continuum (Fardal et al. 2001; see also CO99). These changes to the physical picture reduce the predicted soft X-ray emission by a large factor, and may prove sufficient to reconcile cosmological models with observations without appealing to nongravitational heating mechanisms.

6. SUMMARY

We study the warm-hot intergalactic medium (WHIM), defined as all the gas in the universe with temperature $10^5 < T < 10^7$ K, in six cosmological hydrodynamic simulations with widely varying spatial resolutions, volumes, code algorithms, and input physics. In each simulation, the WHIM contains $\approx$30–40% of all baryons in the present-day universe. As a rule of thumb, our simulations predict that the fractions of baryons in the warm-hot phase, the diffuse phase, and gravitationally bound systems are roughly comparable at the present epoch.

The WHIM comprises primarily gas at moderate overdensities, with a median overdensity of $\sim$10–30, and is predominantly an intergalactic component. It is shock heated by accretion onto nonequilibrium filamentary large-scale structures, with possibly a small energy contribution from nongravitational processes such as supernova feedback. Despite being heated primarily by gravitational processes, WHIM gas in our simulations is consistent with constraints from the soft X-ray background. The clumping factors of WHIM gas in our simulations range from $\sim$30 to 400, which are far below that of virialized objects that some studies assume are the sources of soft XRB photons.

Different simulations give somewhat different fractions of WHIM gas at the present epoch, although the fraction is significant in all simulations. We argue that the differences are primarily attributable to resolution effects, specifically manifested in the distribution of supernova feedback energy in different simulations. In high spatial resolution simulations, the added heat remains in dense regions and radiates away almost immediately, whereas in lower spatial resolution simulations a significant fraction of the heat ends up in diffuse intergalactic gas where it cannot radiate away. Still, the differences in present-day WHIM fraction are not large between these two somewhat extreme cases for feedback. Radiative cooling plays a minor role in the evolution of warm-hot gas because it is mostly at low densities, and is too diffuse to self-gravitate and self-shield into minihalos. Atomic line cooling does, however, play a role in reducing the density of the small fraction of warm-hot gas in the centers of halos. Other physical and numerical effects such as star formation, photoionization, and cosmic variance do not produce significant differences in the amount or properties of warm-hot gas in our simulations.

Since the exact predicted fraction of WHIM gas is as yet sensitive to simulation details, it would be greatly beneficial to place observational constraints on this component. As mentioned before, this is a challenging task. Still, there are tantalizing hints of detections of WHIM gas. Wang & McCray (1993) found an excess emission component in *ROSAT* data around $T \sim 2 \times 10^6$ K, which may be arising from this diffuse component. Soltan et al. (1996) detected an autocorrelation signature between the soft X-ray background and galaxies, as would be expected if warm-hot gas were distributed in large-scale structures. Even more exciting is a possible direct detection by Scharf et al. (2000) of diffuse soft X-ray emission associated with a filament of galaxies. Somewhat stronger evidence comes from a census of O VI absorbers at redshifts $0.14 \lesssim z \lesssim 0.27$ (Tripp et al. 2000; Tripp & Savage 2000), which together with conservative ionization corrections and metallicities implies $\Omega_{\rm WHIM} \gtrsim 0.003^{+0.004}_{-0.002}\ h_{75}^{-1}$, or $\Omega_{\rm WHIM}/\Omega_b \gtrsim 10\%$ at the present epoch. However, some of these O VI absorbers may be photoionized, arising in cooler, low-density intergalactic gas at $T \sim 10^4$ K.

WHIM gas emission may be easiest to detect around high-density regions such as clusters because that is where the density and temperature are highest within the WHIM range (see Fig. 6), but this is *not* where the majority of WHIM gas is located. For instance, high-resolution *Chandra* spectra of regions between clusters that are free of bright sources may provide a detectable signal (L. A. Phillips et al., in preparation), and observations from *XMM* could possibly image filaments of warm-hot gas directly (Pierre, Bryan, & Gastaud 2000). Our simulations, however, predict that the majority of WHIM gas is far away from galaxies and clusters, residing in the diffuse IGM. A promising avenue to detect this more typical WHIM gas is via absorption, as continuing observations with STIS aboard the *Hubble Space Telescope* will detect many more O VI absorbers. Future X-ray satellites may be able to detect higher ionization absorbers such as O VII and O VIII that may also trace WHIM gas (Hellsten, Gnedin, & Miralda-Escudé 1998). The detection of this component is a key observational challenge, since the warm-hot intergalactic medium is rapidly become an integral part of our understanding of the evolution of baryons in the universe.

We thank Rupert Croft, Jeff Gardner, Ed Jenkins, Richard Mushotsky, Arielle Phillips, Jim Peebles, Ue-Li Pen, Todd Tripp, and Kelvin Wu for helpful discussions. R. D. is supported by NASA ATP grant NAG5-7066. R. C. and J. P. O. are supported by NSF grants AST 98-03137 and ASC 97-40300. Support for G. L. B. was provided by NASA through Hubble Fellowship grant HF-01104.01-98A from the Space Telescope Science Institute, which is operated by the Association of Universities for Research in Astronomy, Inc., under NASA contract NAS5-26555. This work was supported by NASA Astrophysical Theory grants NAG5-3922, NAG5-3820, and NAG5-3111, by NASA Long-Term Space Astrophysics grant NAG5-3525, and by the NSF under grants ASC 93-18185, ACI 96-19019, and AST 98-02568. Some of the simulations were performed at the San Diego Supercomputer Center. We also thank NCSA for use of their computing facilities.

REFERENCES

Bahcall, N., Ostriker, J. P., Perlmutter, S., & Steinhardt, P. J. 1999, Science, 284, 1481
Blitz, L., & Robishaw, T. 2000, ApJ, 541, 675
Blitz, L., Spergel, D. N., Teuben, P. J., Hartmann, D., & Burton, W. R. 1999, ApJ, 514, 818
Bryan, G. L. 1999, Comput. Sci. Eng., 1, 46
Cen, R., Miralda-Escudé, J., Ostriker, J. P., & Rauch, M. 1994, ApJ, 437, L9
Cen, R., & Ostriker, J. P. 1999, ApJ, 519, L109 (CO99)
Croft, R. A. C., Di Matteo, T., Davé, R., Hernquist, L., Katz, N., Fardal, M. A., & Weinberg, D. H. 2001, ApJ, submitted (preprint astro-ph/0010345)
Davé, R., Dubinski, J., & Hernquist, L. 1997, NewA, 2, 71
Davé, R., Hernquist, L., Katz, N., & Weinberg, D. H. 1999, ApJ, 511, 521 (DHKW)
Efstathiou, G. 2000, MNRAS, 317, 697
Fardal, M. A., Katz, N., Gardner, J. P., Hernquist, L., Weinberg, D. H., & Davé, R. 2001, ApJ, submitted (preprint astro-ph/0007205)
Fukugita, M., Hogan, C. J., & Peebles, P. J. E. 1998, ApJ, 503, 518
Hellsten, U., Gnedin, N., & Miralda-Escudé, J. 1998, ApJ, 509, 56
Hernquist, L., Katz, N., Weinberg, D. H., & Miralda-Escudé, J. 1996, ApJ, 457, L51
Hui, L., & Gnedin, N. 1997, MNRAS, 292, 27
Kang, H., Ostriker, J. P., Cen, R., Ryu, D., Hernquist, L., Evrard, A. E., Bryan, G. L., & Norman, M. L. 1994, ApJ, 430, 83
Mac Low, M.-M. 2000, in ASP Conf. Ser. 221, Stars, Gas, and Dust in Galaxies, ed. D. Alloin, K. Olsen, & G. Galaz (San Francisco: ASP), in press
Miralda-Escudé, J., Cen, R., Ostriker, J. P., & Rauch, M. 1996, ApJ, 471, 582
Mushotsky, R. F., Cowie, L. L., Barger, A. J., & Arnaud, K. A. 2000, Nature, 404, 459
Pen, U.-L. 1999, ApJ, 510, L1
Persic, M., & Salucci, P. 1992, MNRAS, 258, 14P
Phillips, L. A., Ostriker, J. P., & Cen, R. 2001, ApJ, submitted (preprint astro-ph/0011348)
Pierre, M., Bryan, G., & Gastaud, R. 2000, A&A, 356, 403
Press, W. H., & Schecter, P. 1974, ApJ, 187, 425
Quinn, T., Katz, N., & Efstathiou, G. 1996, MNRAS, 278, 49L
Rauch, M. 1998, ARA&A, 36, 267

Rauch, M., Miralda-Escudé, J., Sargent, W. L. W., Barlow, T. A., Hernquist, L., Weinberg D. H., Katz, N., Cen, R., & Ostriker, J. P. 1997, ApJ, 489, 7
Ryu, D., Ostriker, J. P., Kang, H., & Cen, R. 1993, ApJ, 414, 1
Scharf, C., Donahue, M., Voit, G. M., Rosati, P., & Postman, M. 2000, ApJ, 528, L73
Soltan, A. M., Hasinger, G., Egger, R., Snowden, S., & Truemper, J. 1996, A&A, 305, 17
Thoul, A. A., & Weinberg, D. H. 1996, ApJ, 465, 608
Tripp, T. M., & Savage, B. D. 2000, ApJ, 542, 42
Tripp, T. M., Savage, B. D., & Jenkins, E. B. 2000, ApJ, 534, L1
Tytler, D., Fan, X. M., & Burles, S. 1996, Nature, 381, 207
Wang, Q. D., & McCray, R. 1993, ApJ, 409, L37
Wang, Q. D., & Ye, T. 1996, NewA, 1, 245
Warwick, R. S., & Roberts, T. P. 1998, Astron. Nachr., 319, 59
Wu, K. K. S., Fabian, A. C., & Nulsen, P. E. J. 2000, MNRAS, 318, 889 (WFN00)
Zhang, Y., Anninos, P., & Norman, M. L. 1995, ApJ, 453, L57
Zwaan, M. A., Briggs, F. H., Sprayberry, D., & Sorar, E. 1997, ApJ, 490, 173